Available online at www.sciencedirect.com
SCIENCE DIRECT®
Journal of Nuclear Materials 344 (2005) 173–179
journal of nuclear materials
www.elsevier.com/locate/jnucmat

Thermochemical properties of lanthanides (Ln = La, Nd) and actinides (An = U, Np, Pu, Am) in the molten LiCl–KCl eutectic

Patrick Masset *, Rudy J.M. Konings, Rikard Malmbeck, Jérôme Serp, Jean-Paul Glatz

European Commission, Joint Research Centre, Institute for Transuranium Elements, P.O. Box 2340, 76125 Karlsruhe, Germany

Abstract

The electrochemical reduction of actinides (U, Pu, Np and Am) and lanthanides (La and Nd) chlorides was investigated by cyclic voltammetry and chronopotentiometry at different temperatures in LiCl–KCl eutectic. The diffusion coefficients of these metallic cations were estimated as well as their apparent standard potentials. These values of potentials are compared with existing data measured also by transient electrochemical techniques or e.m.f. measurements.

1. Introduction

The pyrochemical reprocessing represents a promising alternative to the aqueous reprocessing processes to recover minor actinides and fission products from fuel. Electrorefining is envisaged as one process in which the actinides are separated from the bulk of fission products in a molten salt electrolyte by electrotransport. For this reason, the assessment of accurate electro- and thermochemical data of actinides as well as those of lanthanides is of high importance. The first reliable studies of electrochemical properties of actinides in molten salts started at the end of 50s with the properties of uranium [1–3]. Thereafter, the electrochemical behaviour of plutonium-based solutions in molten chlorides was also investigated [4,5]. Martinot [6] reported standard potentials for the actinide redox systems of U, Pu, Am, Np and Cm. However, these results are subject to doubts. In the last years, a reassessment of the thermochemical properties of actinide chlorides in the LiCl–KCl eutectic has been carried out: U [7–9], Pu [7,10], Am [7,11,12], Np [7,13]. Also at ITU, a systematic investigation of actinide-based solutions in the LiCl–KCl has been carried out. This paper gives an overview of the results obtained up to now.

2. Experimental

2.1. Chemicals

Anhydrous LiCl–KCl eutectic (+99.99% purity), Bi metal (+99.99% purity), anhydrous $BiCl_3$, $LaCl_3$ and $NdCl_3$ (+99.9% purity) were purchased from Aldrich and used as received. Silver chloride (99.9% purity, Aldrich) and silver wire of 1 mm diameter (99.99% purity, Alfa Aesar) were used for the reference electrode. Other

* Corresponding author. Tel.: +49 7247 951 152; fax: +49 7247 951 593.
E-mail address: patrick.masset@cec.eu.int (P. Masset).

0022-3115/$ - see front matter © 2005 Elsevier B.V. All rights reserved.
doi:10.1016/j.jnucmat.2005.04.038

electrode materials, molybdenum and tungsten metals (+99.95% purity), were purchased from Alfa Aesar. The Mo and W wires (1 mm in diameter) were washed before use in dilute hydrofluoric acid and rinsed in deionised water and then in ethanol.

$AnCl_3$ were prepared directly in the LiCl–KCl melt by oxidising the corresponding metal. The actinide metals come from the ITU stock material (plutonium: ^{239}Pu-95%–^{240}Pu-4.6%, low Am content, uranium: depleted U, americium: high purity ^{241}Am, >99%). The actinide metal was introduced in a molten metallic pool (Cd or Bi) in the bottom of the crucible, and then oxidised by adding either $CdCl_2$ or $BiCl_3$ in the salt phase. The exchange reaction (1) between the metallic and the salt phases occurs as follows [10]:

$$n\mathrm{An}^0\ (\text{metallic-phase}) + 3\mathrm{M}^{n+}\ (\text{salt-phase}) \Longleftrightarrow n\mathrm{An}^{3+}\ (\text{salt-phase}) + 3\mathrm{M}^0 \quad (1)$$

where M denotes metallic element (M = Cd, Bi) and n is the oxidation state of M in the salt phase. By this method, a quantified amount of An^{3+} could be released in the salt phase.

For neptunium-based experiments, $NpCl_4$ was the starting material (from ITU stock). However, it was found that the 4+ state was not stable with time in the LiCl–KCl bath. Therefore, it was first reduced to Np metal by adding quantitatively Bi–Li alloy (Li content: 35 mol%) in the LiCl–KCl bath. The reduction step was carried out at 500 °C, above the Li–Bi melting point [14]. Then, the previous procedure was applied to obtain a solution of $NpCl_3$. As the $NpCl_4$ was reduced quantitatively by the Li–Bi alloy, the $BiCl_3$ added is dedicated only to the oxidation of the Np metal into Np^{3+} according to Eq. (1).

2.2. Apparatus

The electrochemical experiments, storage and handling of all chemicals were carried out in a glove box under purified argon atmosphere (less than 5 ppm of water and 10 ppm of oxygen). The glove box was equipped with a well-type oven in which the experimental set-up could be moved up and down using a lift system. A Eurotherm controller combined with a chromel–alumel thermocouple in an Al_2O_3 sheath maintained the melt temperature with an estimated accuracy of ±2 °C. The electrodes and the thermocouple were positioned through a water-cooled top flange, which supported the alumina or quartz crucible used in the electrochemical cell (Fig. 1).

The working electrode consisted of a metallic tungsten (W) wire (1 mm diameter) dipped into the bath. The active electrode surface was determined after each experiment by measuring the immersion depth of the electrode in the molten salt. The auxiliary electrode was made of molybdenum (Mo) wire (1 mm diameter) bent into a spiral shape. Silver–silver chloride (1 wt%, or $X_{AgCl} = 0.0039$ molar fraction, AgCl in LiCl–KCl) was used as reference electrode [15,16]. The silver wire, an alumina tube sheath, as well as the AgCl (1 wt%)–LiCl–KCl salt were placed in a thin Pyrex® (Duran) tube and dipped in the solution.

2.3. Techniques

2.3.1. Electrochemical techniques

Transient electrochemical techniques, i.e. cyclic voltammetry (CV) and chronopotentiometry (CP), were carried out in an electrochemical cell having a three-electrode set-up. The measurements were realised with a Princeton Applied Research PAR 273 potentiostat

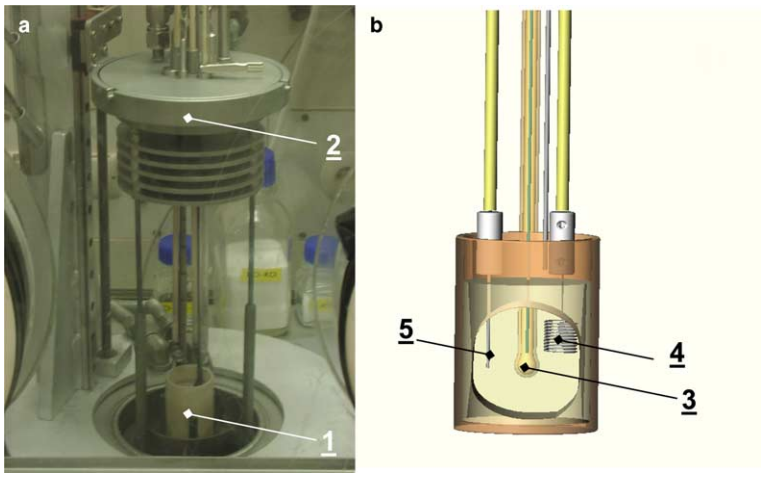

Fig. 1. (a) Experimental set-up in the glove box, (b) details of the electrochemical cell arrangement; (1) crucible, (2) cooled flanged and lifting system, (3) Ag/AgCl reference electrode, (4) spiral shaped Mo wire counter electrode, (5) W working electrode.

with an EG&G M270 electrochemical software. For semi-integral analysis of cyclic voltammograms by the convolution method (Conv), the Condecon software was used.

2.3.2. Analysis and characterisation techniques

Samples (about 100 mg) were taken from the salt phase and dissolved in 1 M nitric acid. The concentration of actinide and the isotopic ratio were determined by ICP-MS analysis and by non-destructive analysis specially developed for pyrochemical samples [17,18].

3. Results and discussion

3.1. Electrochemical determinations

Fig. 2 shows typical cyclic voltammograms obtained at 460 °C with actinide-based solutions superimposed to the blank experiment done with the LiCl–KCl eutectic. The electroreduction of Pu^{3+} [10], U^{3+} [8,9,19], Np^{3+} [13] ions to metal proceeds via a one-step process. The electroreduction of Am^{3+} proceeds via a two-step mechanism involving Am^{2+} [20,21]. Signals for U^{4+}/U^{3+} (~−0.25 V vs Ag/AgCl, 460 °C) and Np^{4+}/Np^{3+} (~0.3 V vs Ag/AgCl, 460 °C) redox systems can be observed at more anodic potentials. In Fig. 2, cyclic voltammograms of lanthanum and neodynium-based solutions are compared with americium-based one. Lanthanum is reduced via an one-step process ($E_{p,c}$ ~ −2.07 V vs Ag/AgCl, 460 °C). The reduction of neodynium trichloride takes place in two steps involving Nd^{2+} [22,23].

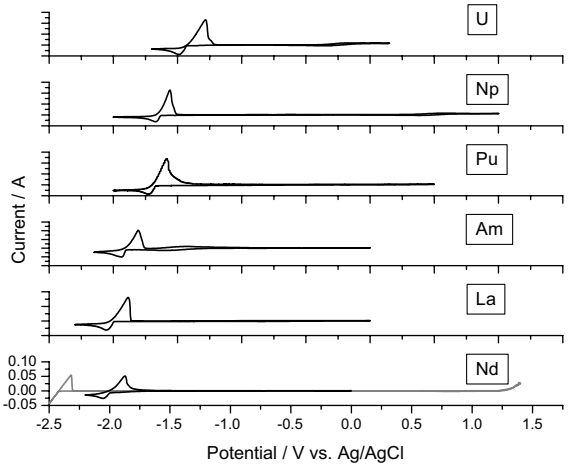

Fig. 2. Comparative cyclic voltammograms obtained on W electrode for actinides in LiCl–KCl eutectic salt (grey line). $T = 733$ K, reference electrode Ag/AgCl (1 wt%), $[Am^{3+}] = 3.65 \times 10^{-5}$ mol cm^{-3} and $S = 0.2$ cm^2, $[Pu^{3+}] = 8.3 \times 10^{-5}$ mol cm^{-3} and $S = 0.2$ cm^2, $[U^{3+}] = 9.87 \times 10^{-5}$ mol cm^{-3} and $S = 0.34$ cm^2, $[Np^{3+}] = 10.3 \times 10^{-5}$ mol cm^{-3} and $S = 0.063$ cm^2, $[La^{3+}] = 20 \times 10^{-5}$ mol cm^{-3} and $S = 0.19$ cm^2, $[Nd^{3+}] = 70 \times 10^{-5}$ mol cm^{-3} and $S = 0.24$ cm^2.

3.1.1. Diffusion coefficients

The diffusion coefficients were estimated at different temperatures from data obtained with chronopotentiometry, cyclic voltammetry and convolution. From CP measurements, the diffusion coefficients were calculated using the Sand's equation [24].

$$i\sqrt{\tau} = 0.5n\ FC_{M^{n+}}S\sqrt{\pi D_{M^{n+}}}. \quad (2)$$

The linear relationship between i and $\tau^{-1/2}$ was verified for every temperature and concentration. The diffusion coefficient was also determined from cyclic voltammetry using the Randles–Sevick equation [25]:

(i) for a soluble–insoluble transition

$$I_p/\sqrt{v} = 0.446(nF)^{3/2}(RT)^{-1/2}C_{M^{n+}}SD_{M^{n+}}^{1/2}, \quad (3)$$

(ii) for insoluble–soluble transition

$$I_p/\sqrt{v} = 0.61(nF)^{3/2}(RT)^{-1/2}C_{M^{n+}}SD_{M^{n+}}^{1/2}. \quad (4)$$

In addition, the convoluted current was calculated as proposed by Savéant et al. [26]:

$$m = 1/\pi^{1/2}\int_0^t i(u)/(t-u)^{1/2}\mathrm{d}u, \quad (5)$$

where the limiting value m^* is equal to:

$$m^* = 3FSC_{M^{n+}}\sqrt{D_{M^{n+}}}. \quad (6)$$

Plotting the diffusion coefficients against the inverse of the absolute temperature, straight lines were obtained. It follows Arrhenius-type law:

$$D = D^0\exp(-E_a/RT), \quad (7)$$

where D^0 is the pre-exponential factor, E_a is the apparent activation energy (kJ mol^{-1}) and T the absolute temperature. Diffusion coefficient values obtained at 450 °C are summarised in Table 1.

3.1.2. Apparent standard potentials

From CP measurements, and for a reversible insoluble–soluble transition, the apparent standard potential was calculated as follows [25,27]:

$$E = E_{1/2}^{insol-sol} + \frac{RT}{(p-q)F}\cdot\ln\left(\frac{\tau^{1/2}-t^{1/2}}{\tau^{1/2}}\right), \quad (8)$$

where p and q are the oxidation states of the oxidised and reduced forms, respectively and $E_{1/2}^{insol-sol}$ is equal to:

$$E_{1/2}^{insol-sol} = E^{0^*}(M^{p+}/M^{q+}) + \frac{RT}{(p-q)F}\cdot\ln(X_{M^{p+}}) \quad (9)$$

and $X_{M^{p+}}$ is the molar fraction of the M^{p+} species.

Table 1
Diffusion coefficients of $AnCl_x$ and $LnCl_x$ in the molten LiCl–KCl eutectic at 450 °C

	$10^5\ D/cm^2\ s^{-1}$
UCl_3	2.7 ± 0.2
UCl_4	2.1 ± 0.2
$NpCl_3$	1.7 ± 0.2
$PuCl_3$	1.6 ± 0.1
$AmCl_2$	1.1 ± 0.1
$AmCl_3$	2.5 ± 0.2
$NdCl_3$	1.1 ± 0.1
$LaCl_3$	0.8 ± 0.1

From CV experiments, the apparent standard potential was calculated from the peak potentials. For a reversible insoluble–soluble system, the cathodic potential peak can be expressed as follows [28,29]:

$$E_{p,c} = E^{0^*}(M^{p+}/M^{q+}) + \frac{RT}{(p-q)F}\cdot\ln(X_{M^{p+}}) - 0.854\cdot\frac{RT}{(p-q)F}. \quad (10)$$

In case of a reversible soluble–soluble transition, the half-peak potential is used and the expression becomes [25]:

$$E_{p/2} = E_{1/2}^{sol-sol} + 1.09\frac{RT}{(p-q)F}, \quad (11)$$

where $E_{1/2}^{sol-sol}$ is the half wave potential.

$$E_{1/2}^{sol-sol} = E^0_{M^{p+}/M^{q+}} + \frac{RT}{(p-q)F}\cdot\ln\left(\frac{\gamma_{M^{p+}}}{\gamma_{M^{q+}}}\right) + \frac{RT}{nF}\cdot\ln\left(\frac{\sqrt{D_{M^{q+}}}}{\sqrt{D_{M^{p+}}}}\right). \quad (12)$$

The apparent standard potential could be expressed as follows:

$$E^{0^*}_{M^{p+}/M^{q+}} = E^0_{M^{p+}/M^{q+}} + \frac{RT}{(p-q)F}\cdot\ln\left(\frac{\gamma_{M^{p+}}}{\gamma_{M^{q+}}}\right). \quad (13)$$

In addition, apparent standard potentials were derived from semi-integration of the voltammograms. For a reversible insoluble–soluble redox system, the logarithmic analysis of the wave permits the calculation of the values of $E^{0^*}_{M^{p+}/M^{q+}}$ using (14). The potential is expressed as a function of the convoluted current m [26].

$$E = E_{1/2}^{insol-sol} + \frac{RT}{(p-q)F}\cdot\ln\left(\frac{m^*-m}{m^*}\right). \quad (14)$$

In case of a reversible soluble–soluble redox system, the expression differs as follows [26]:

$$E = E_{1/2}^{sol-sol} + \frac{RT}{(p-q)F}\cdot\ln\left(\frac{m^*-m}{m}\right), \quad (15)$$

$E_{1/2}^{sol-sol}$ and $E_{1/2}^{insol-sol}$ have the same meaning as previously.

On the basis of the slope of the curve E vs $\ln[(m^*-m)/m^*]$ or E vs $\ln[(m^*-m)/m]$, the number of electrons exchanged during the redox process were estimated. One-electron and two-electron processes were found for the Am^{3+}/Am^{2+} and Am^{2+}/Am^0 transitions, respectively. It confirms that the electroreduction of $AmCl_3$ to Am metal proceeds via a two-step mechanism. The same behaviour was noticed for $NdCl_3$, which also shows multiple valency. Apparent standard potentials of the An^{3+}/An^0 and Ln^{3+}/Ln^0 transitions (except for americium: Am^{2+}/Am^0 [20,21] and neodymium: Nd^{2+}/Nd^0 [22,23]) vs the temperature are reported in Fig. 3. For most elements, a good agreement with literature data is observed, except for americium. The differences is likely due to the technique used, e.m.f. measurements are hampered by the disproportionation reaction of americium metal with Am^{3+} which may change the actinide concentration in the bath.

3.2. Thermodynamics calculations

The standard Gibbs energy of formation, $\Delta G^\infty(MCl_x)$ at infinite dilution is calculated according the following equation:

$$\Delta G^\infty(MCl_x) = -(p-q)FE^{*0}(M^{p+}/M^{q+}). \quad (16)$$

Apparent standard potentials were derived from electrochemical measurements. Plotting values of the apparent standard potential vs the absolute temperature, a linear dependence was obtained. Therefore, the free Gibbs energy of formation $\Delta G^\infty(MCl_x)$ can be expressed as follows:

$$\Delta G^\infty(MCl_x) = \Delta H^\infty(MCl_x) - T\Delta S^\infty(MCl_x), \quad (17)$$

where $\Delta H^\infty(MCl_x)$ and $\Delta S^\infty(MCl_x)$ are respectively the enthalpy and the entropy of formation at infinite dilute

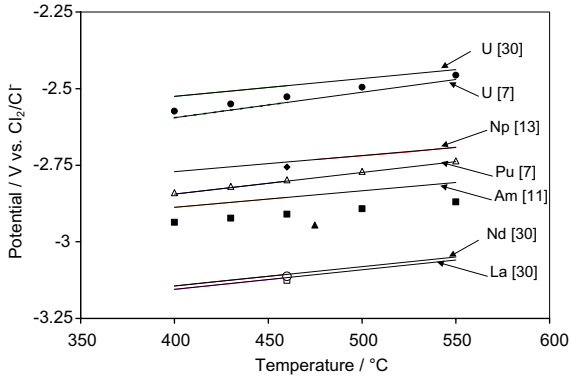

Fig. 3. Evolution of the apparent standard potential vs the temperature, (●) U this work, (♦) Np this work, (△) Pu this work, (■) Am this work, (○) Nd this work, (□) La this work, (black lines) literature values, (▲) Am, $T = 470$ °C [21].

Table 2
The selected thermodynamic properties for $AnCl_x$ and $LnCl_x$ compounds

	$\Delta_f H^0$/kJ mol^{-1}	S^0/J K^{-1} mol^{-1}	C_p (cr)/J K^{-1} mol^{-1}	T_{fus}/K	$\Delta_{fus}H^0$/ kJ mol^{-1}	C_p (liq.)/ J K^{-1} mol^{-1}
UCl_3	− 863.7 ± 2.5	163.9 ± 0.5	$87.779 + 31.12\times10^{-3}\,(T/K) + 458.33\times10^{3}/(T/K)^{-2}$	1115	49	150
UCl_4	− 1019.8 ± 2.5	197.2 ± 0.8	$106.854 + 48.65\times10^{-3}\,(T/K) - 89.603\times10^{3}/(T/K)^{-2}$	863	49.8	162.34
$NpCl_3$	−896.8 ± 2.5	165.2 ± 0.8	$89.598 + 27.5\times10^{-3}\,(T/K) + 83.712/(T/K)^{-2}$	1075	50	137
$PuCl_3$	−959.6 ± 2.5	161.4 ± 0.8	$91.412 + 37.16\times10^{-3}\,(T/K) + 27.38\times10^{3}/(T/K)^{-2}$	1041	49	144
$AmCl_2$	−654.0 ± 2.5	148.1 ± 0.8	(α phase) $64.992 + 24.57\times10^{-3}\,(T/K) + 250.068\times10^{3}/(T/K)^{-2}$	1221	17.2	110
			(β phase) 124	1114	15.8	
$AmCl_3$	−977.8 ± 2.5	146.2 ± 0.8	$81.811 + 41.29\times10^{-3}\,(T/K) + 337.81\times10^{3}/(T/K)^{-2}$	991	48.1	144
$NdCl_3$	−1040.9 ± 1.0	153.43 ± 0.5	$87.2834 + 38.5855\times10^{-3}\,(T/K) + 0.04021\times10^{6}/(T/K)^{-2}$	1032	47.7	149.5
$LaCl_3$	−1071.6 ± 1.5	137.47 ± 0.5	$74.9288 + 51.6544\times10^{-3}\,(T/K) + 0.68452\times10^{6}/(T/K)^{-2}$	1133	48.5	157.7

Table 3
Apparent standards potentials free Gibbs energies of formation and activity coefficients of $AnCl_x$ and $LnCl_x$ in the molten LiCl–KCl eutectic

		T/K	E^{0*} V vs Ag/AgCl	E^{0*} V vs Cl_2/Cl^-	$\Delta G^{\infty}_{MCl_x}$, kJ mol^{-1}	$10^3\times\gamma^0$
Uranium	UCl_3	673	−1.360	−2.576	−745.13	0.29
		703	−1.341	−2.563	−741.83	0.35
		773	−1.274	−2.563	−726.20	1.39
		823	−1.218	−2.462	−712.85	4.47
	UCl_4	673	−0.275	−1.491	−143.95	17.1
		703	− 0.251	−1.473	−142.12	16.3
		773	− 0.194	−1.428	−137.80	14.8
		823	− 0.157	−1.400	−135.18	12.7
Neptunium	$NpCl_3$	733	−1.530	−2.756	−797.9	0.004
Plutonium	$PuCl_3$	733	−1.5702	−2.7962	−809.5	3.5
		773	−1.5336	−2.7699	−801.9	5.0
		823	−1.4906	−2.7361	−792.1	7.9
Americium	$AmCl_3$	733	−1.4693	−2.6953	−821.9	4.7
		773	−1.4393	−2.6756	−816.6	5.1
		823	−1.3877	−2.6332	−808.3	7.2
	$AmCl_2$	733	−1.6854	−2.9114	−561.9	2.7
		773	−1.6564	−2.8927	−558.3	3.8
		823	−1.6265	−2.8720	−554.3	5.2
Neodymium	$NdCl_3$	733	−1.907	−3.113	−901.2	0.08
	$NdCl_2$	733	−1.846	−3.073	−889.6	–
Lanthanum	$LaCl_3$	733	−1.900	−3.126	−904.9	5.7

solution. The activity coefficients of MCl_x, γ_{MCl_x}, in the LiCl–KCl eutectic were calculated using Eq. (18) from the difference between the Gibbs energy of formation at infinite dilution (determined from electrochemical measurements) and the Gibbs energy of formation in the supercooled state (sc) taken as reference state.

$$RT\ln\gamma(MCl_x) = \Delta G^{\infty}(MCl_x) - \Delta G^{0}_{sc}(MCl_x). \quad (18)$$

The Gibbs energy of formation of MCl_x in the supercooled state was derived from the crystal data (cr) of MCl_x (cr), the enthalpy of fusion ($\Delta_{fus}H$) and the heat capacity of the liquid phase (C_p) [30] according to Eq. (19). The selected thermodynamic data are summarised in Table 2.

$$\begin{aligned}\Delta G^{0}(MCl_n, l) = {} & \Delta H^{0}(MCl_n, f, 298.15\,K) \\ & - T\Delta S^{0}(MCl_n, f, 298.15\,K) \\ & + \int_{298.15}^{T_m} \Delta C_p(MCl_n, s)\mathrm{d}T \\ & + T\int_{298.15}^{T_m} \frac{\Delta C_p(MCl_n, s)}{T}\mathrm{d}T \\ & + \int_{T_m}^{T} \Delta C_p(MCl_n, l)\mathrm{d}T \\ & + T\int_{T_m}^{T} \frac{\Delta C_p(MCl_n, l)}{T}\mathrm{d}T \\ & + \Delta H_m\left(1 - \frac{T}{T_m}\right). \end{aligned} \quad (19)$$

The Gibbs energy of formation of MCl_x in the supercooled state was derived from the crystal data (cr) of MCl_x (cr), the enthalpy of fusion ($\Delta_{fus}H$) and the heat capacity of the liquid phase (C_p) [30]. The selected thermodynamic data are summarised in Table 2.

The expressions of the free Gibbs energy of $\Delta G^{\infty}(MCl_x)$, deduced from the potential measurements are (see values in Table 3):

- Uranium chlorides UCl_3 and UCl_4 [19]:

$$\Delta G^{\infty}(UCl_3) = -897.09 + 0.2226\ T(K)/\mathrm{kJ\ mol^{-1}},$$
$$\Delta G^{\infty}(UCl_4) = -183.53 + 0.0589\ T(K)/\mathrm{kJ\ mol^{-1}}.$$

- Plutonium trichloride $PuCl_3$ [10]:

$$\Delta G^{\infty}(PuCl_3) = -956.6 + 0.200\ T(K)/\mathrm{kJ\ mol^{-1}}.$$

- Americium chlorides $AmCl_3$ and $AmCl_2$ [12]:

$$\Delta G^{\infty}(AmCl_3) = -933.7 + 0.152\ T(K)/\mathrm{kJ\ mol^{-1}},$$
$$\Delta G^{\infty}(AmCl_2) = -623.9 + 0.085\ T(K)/\mathrm{kJ\ mol^{-1}}.$$

For $NpCl_3$, $LaCl_3$ and $NdCl_3$ data obtained at 733 K are reported in Table 3. The activity coefficients calculated at different temperatures range between 10^{-6} and 5×10^{-3}.

4. Conclusions

The thermochemical properties of lanthanides (Ln = La, Nd) and actinides (An = U, Pu, Am, Np) in the molten LiCl–KCl eutectic were investigated by means of transient electrochemical techniques. This approach allows the determination of accurate values of standard potentials, also for multi-valency elements such americium and neodymium. In addition, the diffusion coefficients, the free Gibbs energies of formation, and the activity coefficients were derived from the electrochemical measurements. For apparent standard potential values, a good agreement was obtained with the literature data, except for americium.

References

[1] D. Inman, G.J. Hills, L. Young, J.O'M. Bockris, Trans. Faraday Soc. 79 (11) (1959) 1904.
[2] D.L. Hill, J. Perano, R.A. Osteryoung, J. Electrochem. Soc. 107 (8) (1960) 698.
[3] D.M. Gruen, R.A. Osteryoung, Ann. NY Acad. Sci. 79 (11) (1960) 897.
[4] A. Leseur, Report CEA-R-3793, 1969.
[5] D.A. Nissen, Report BNWL, 1965.
[6] L. Martinot, J. Inorg. Nucl. Chem. 37 (1975) 2525.
[7] J.J. Roy, L.F. Granthman, D.L. Grimett, S.P. Fusselman, C.L. Krueger, T.S. Storvick, T. Inoue, Y. Sakamura, N. Takahashi, J. Electrochem. Soc. 143 (8) (1996) 2487.
[8] B.P. Reddy, S. Vandarkuzhali, P. Venkatesh, Electrochim. Acta 49 (2004) 2471.
[9] O. Shirai, T. Iwai, Y. Suzuki, Y. Sakamura, H. Tanaka, J. Alloys. Compd. 271 (1998) 685.
[10] J. Serp, R.J.M. Konings, R. Malmbeck, J. Rebizant, C. Scheppler, J.P. Glatz, J. Electroanal. Chem. 561 (2004) 143.
[11] S.P. Fusselman, J.J. Roy, D.L. Grimett, L.F. Granthman, C.L. Krueger, C.R. Nabelek, T.S. Storvick, T. Inoue, T. Hijikata, K. Kinoshita, Y. Sakamura, K. Uozumi, T. Kawai, N. Takahashi, J. Electrochem. Soc. 146 (7) (1999) 2573.
[12] J. Serp, P. Chamelot, S. Fourcaudot; R.J.M. Konings, R. Malmbeck, C. Pernel, J.C. Poignet, J. Rebizant, J.P. Glatz, Electrochim. Acta, in press.
[13] O. Shirai, M. Iizuka, T. Iwai, Y. Arai, J. Appl. Electrochem. 31 (2001) 1055.
[14] J. Sangster, A.D. Pelton, in: H. Okamoto, P.R. Sabramanian, L. Kacparack (Eds.), Binary Alloy Phase Diagram, 2nd Ed., vol. 1, 1990, p. 757.
[15] R. Littlewood, Electrochim. Acta 3 (1961) 270.
[16] L. Yang, R.G. Hudson, J. Electrochem. Soc. 106 (11) (1959) 986.
[17] S. Abousahl, P. van Belle, H. Eberle, H. Ottmar, B. Lynch, P. Vallet, K. Mayer, M. Ougier, Radiochem. Acta 93 (3) (2005) 147.
[18] S. Abousahl, P. van Belle, H. Eberle, H. Ottmar, K. Mayer, P. Ragan, M. Ougier, J. Serp, in: Proceedings of Atalante, Avignon, 2004.
[19] P. Masset, P.D.W. Bottomley, R. Malmbeck, A. Rodrigues, J. Serp, J.P. Glatz, J. Electrochem. Soc. 152 (6) (2005) A1109.
[20] J. Serp, R. Malmbeck, E. Yakub, J.P. Glatz, in: Proceedings of the Global, 2003.
[21] D. Lambertin, J. Lacquement, S. Sanchez, G.S. Picard, Plasma Ions 3 (2000) 65.

[22] C. Pernel, J. Serp, M. Ougier, R. Malmbeck, J.P. Glatz, in: Proceedings of the Global, 2001.
[23] Y. Mottot, PhD thesis, Univ. Paris VI, 1986.
[24] H.J.S. Sand, Philos. Mag. 1 (1901) 45.
[25] A.J. Bard, L.R. Faulkner, in: Fundamentals and Applications, Wiley, New York, 1980.
[26] J.C. Imbeaux, J.M. Savéant, Electroanal. Chem. Interfacial Electrochem. 44 (1973) 169.
[27] P. Delahay, in: New Instrumental Methods in Electrochemistry, Interscience, New York, 1954.
[28] Y. Castrillejo, M.R. Barmejo, E. Barrado, A.M. Martinez, P. Diaz Arocas, J. Electroanal. Chem. 545 (2003) 141.
[29] T. Berzins, P. Delahay, J. Am. Chem. Soc. 75 (1953) 555.
[30] R.J.M. Konings (www.f-elements.net) 2002.